Analysis of Numerically Simulated True Strain on High Stampability Sheets

Heber Castro Silva
hebercs@uol.com.br

Sérgio Fernando Lajarin
espanhol@ufpr.br

Paulo Victor P. Marcondes
marcondes@ufpr.br
Federal University of Paraná – UFPR
Dept. of Mechanical Engineering
C.P. 19011
81530-900 Curitiba, PR, Brazil

The sheet metal forming is a manufacturing process widely used industrially. The quality and efficiency of the process is dependent on the correct choice of the process parameters and the correct understanding of the sheet metal behavior. The identification of the regions where stretching and/or deep drawing occurred during the forming process can aid the process through the tools design optimization. This work consisted of evaluating three punch models with varied geometries. The purpose of this work was to simulate different punch geometries using the ANSYS/LS_DYNA program and to compare the results with those reported in the literature. An evaluation was also made of the chosen program's response quality (validation). The material model chosen was the Barlat's model. The friction coefficient influence was also investigated. A comparison of the major true strain (ε1) obtained by simulation compared with the experimental results indicated that this material model is able to satisfactorily reproduce the major true strain found in practice for the DC 06 steel.
Keywords*: stamping, tool geometry, modeling, finite element analysis*

Introduction

Stamping tools are traditionally designed by professionals with practical experience who can determine the best stamping process configuration for each shape based on the use of tryout techniques, the circle grid analysis method and the Forming Limit Curve – FLC (Hongzhi and Zhongqin, 2000; Cao et al., 2000). Even so, after the tooling has been built, adjustments are needed before it is finalized and handed over to production.

Predicting tool behavior through numerical simulation is an important design tool, since it allows reducing the number of practical tests to be carried out prior to the tool's completion and delivery to the client. Simulation also allows one to predict the critical strain areas in workpieces, allowing modifications to be made in the dies, or even in the product, while still in the design phase. Moreover, analytical or experimental solutions that can easily describe all the possible strains pathways for this type of operation are almost impossible (Yao and Cao, 2002).

The material's Forming Limit Curve, which can be obtained from Nakazima's stamping test (Nakazima et al., 1968), corresponds to the geometrical location of the maximum true strain points of a sheet subjected to stretching, deep drawing and/or plane strain condition. The knowledge of the FLC curve is essential so that the strains produced during industrial stamping processes do not exceed a safe percentage of true strain, thus ensuring the final workpiece quality. Today researches are focused on perfecting Nakazima's test tools in order to obtain results that are closer to reality, characterizing in the best possible way the phenomena acting during large plastic deformation (Sampaio et al., 1998; Yao and Cao, 2002). Therefore, the test in its traditional form and as a modified version will be modeled using LS-Dyna software and the data obtained compared with the results reported by Chemin Filho (2004) and Chemin Filho and Marcondes (2008).

The purpose of this work is to investigate the influence of some parameters in the sheet metal forming simulation, as well as the ability of the material model and the software to accurately represent the actual strain modes, i.e., to represent the critical strain and strain distribution on stamping processes. An analysis is also made of the lubrication influence on the forming process.

Paper accepted December, 2009. Technical Editor: Anselmo Eduardo Diniz

Nomenclature

E = *modulus of elasticity*
EPTO1 = *major true strain*
EPTO2 = *minor true strain*
FLC = *forming limit curve*
K = *plastic resistance constant*
m = *Centered Body Cubic coefficient*
R1 = *punch head radius*
R2 = *external congruence radius*
R0 = *anisotropy coefficient at 0°*
R45 = *anisotropy coefficient at 45°*
R90 = *anisotropy coefficient at 90°*

Greek Symbols

ε1 = *major true strain*
ε2 = *minor true strain*
ρ = *density*
ν = *poisson's coefficient*
μ = *friction's coefficient*

Experimental Methodology

A series of experiments using the test proposed by Nakazima et al. (1968) were conducted by Chemin Filho (2004) to ascertain the Forming Limit Curve for the 0.7 mm thick DC 06 steel (according to the DIN 10152 standard). In addition to the punch geometry normally used in the Nakazima's test, other geometries were tested in order to study their influence on the material's stampability response (Borsoi, 2000).

In this work, to reproduce the experiments presented by Chemin (2004) and to evaluate the ability of the LS-Dyna software to reproduce these results, various experiments were carried out following the methodology described below and reported in earlier works (Moreno, 2000; Evangelista, 2000 and Costa, 2003).

Preprocessing

This phase consisted of analyzing the data required in the preprocessing phase, such as the tools' geometries, material characteristics and loading types (Chemin Filho, 2004). The representative experiment model was built (Fig.1). The punch and die modeling was made using the ANSYS 9.0/LS_DYNA program.

Due to the symmetry of the problem, only one quarter of the geometry of each component was built. Due to a simple shape part it was chosen the forming limit strain diagram instead of the forming limit stress diagram – independently on strain path – (Gronostajski et al., 2004).

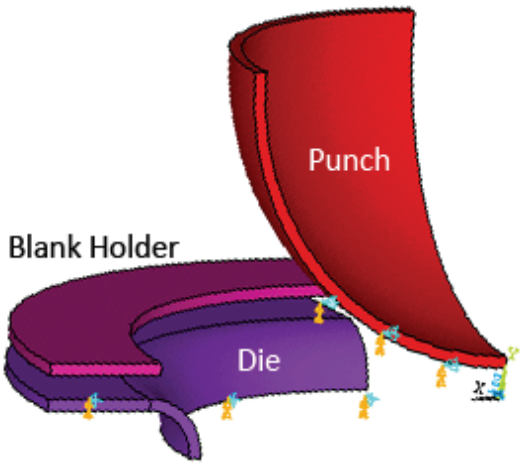

Figure 1. Punch and die modeling.

The punch and die were defined as rigid bodies. This type of definition allows that all the nodes freedom degrees could be connected to its gravity center so that the number of the rigid body freedom degrees is limited to six, independently of the number of nodes. The downward velocity of the punch used here was 400 mm/s.

Two types of elements were used to model the Nakazima's test: the shell type to model the sheet, and the solid type to model the punch, die and blank holder. A detailed description of these elements formulation is given in Hallquist (1998).

The following options were used for the shell elements:

- S/R Hughes-Liu type formulation: This is a formulation similar to that of Hughes-Liu, but with selective reduced integration. This formulation requires greater computational resources but prevents certain modes of instability.
- Number of integration points in the direction of thickness equals to five.
- Integration rule: Gauss quadrature.
- Nodal distance: 2.5 mm, when local refinement of the grid was not indicated, and 0.8 mm, when local refinement was indicated.

The material tested experimentally by Chemin Filho (2004) was characterized as anisotropic. Among the available models in the LS-Dyna software to specify this material type the Barlat's one was selected (Barlat and Lian, 1989).

Because the material's structure is Centered Body Cubic, the *m* coefficient selected was 6 (Abrantes and Batalha, 2003). The material properties are listed in Table 1.

Table 1. DC 06 main properties.

Property	Value	Unit	Source
Density (ρ)	7.850	g/cm^3	Literature
Modulus of Elasticity (E)	210	GPa	Literature
Poisson's Coefficient (ν)	0.3	(dimensionless)	Literature
Plastic Resistance Constant (K)	626.8	MPa	Tension Test
m	6	(dimensionless)	Literature
Anisotropy Coefficient at 0° (R_0)	2.0483	(dimensionless)	(Chemin, 2004)
Anisotropy Coefficient at 45° (R_{45})	1.8659	(dimensionless)	(Chemin, 2004)
Anisotropy Coefficient at 90° (R_0)	2.5988	(dimensionless)	(Chemin, 2004)

Processing

The model was simulated using LS-Dyna software. In the case of the 50 mm radius punch, different friction coefficient values were tested, and the value providing the best curve fit in relation to the experimental data was used in the other cases (validation).

Post-Processing

In order to compare the data obtained and the experimental data reported by Chemin Filho (2004), the major true strain curves (ε_1) obtained by simulation and experiment were plotted.

Materials and Methods

Thin square 200 mm-sided sheets were used as test specimens, as well as three punch geometries. The first punch was cylindrical, with a flat bottom and 10 mm radius. The purpose of this punch is to generate preferentially deep drawing phenomena due to its cylindrical shape and its large initial contact area with the sheet. The second punch had a hemispherical shape and a 50 mm radius (corresponding to the original shape for the Nakazima's test). The third punch had a deep-ellipse shape (25 mm radius) and ideally favors stretching strains. All the punch models had a 100 mm diameter, following the dimensions proposed by Nakazima et al. (1968) (Fig. 2).

Results and Discussion

Analysis of the True Strain Distribution with the Hemispherical Punch (Rp 50 mm)

Figure 3 illustrates the major true strain distribution (ε_1) as a function of the distance from the punch center (punch pole) for different friction coefficients, i.e., between 0.0 and 0.20. Chemin's (2004) experimental values without the lubricant addition are also presented.

In the zero friction condition, the strain distribution reached a maximum value close to the pole (node number 1372) decreasing, as it goes further away from that region.

With a friction coefficient other than zero, the contact with the punch restrains the sheet movement. It can be observed that the ε_1 presents a deviation from the punch center as the friction coefficient increases. Because the strain distribution in the region of contact with the die is also restricted both by the blank holder and by the friction with the die, the region of maximum true strain is now the region in contact neither with the punch nor the die. Lobão (2003) observed this same effect.

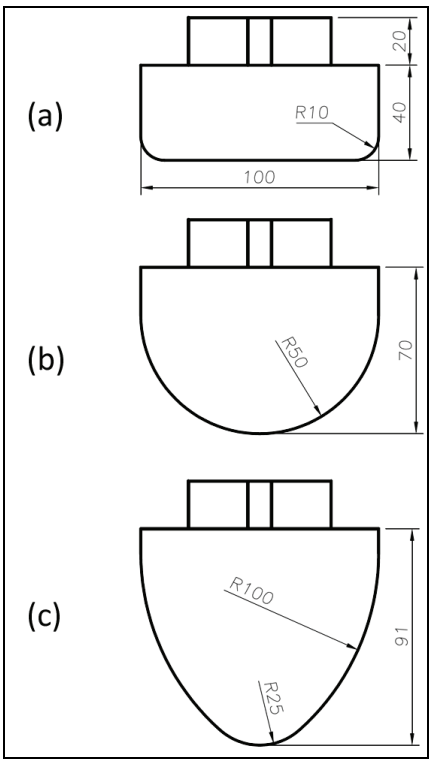

Figure 2. Punch Models (adapted from Chemin Filho, 2004): a) flat punch (Rp 10 mm), b) hemispherical punch (Rp 50 mm) and c) deep-ellipse punch (Rp 25 mm).

Figure 3 also shows that the simulated values for a friction coefficient of 0.15 are in good agreement with the experimental values in the region of maximum true strain between the die and the punch radii. In the region corresponding to the pole of the punch, the experimental values (ε_1) were slightly lower than those found for this friction value.

It can be noted (Fig. 4a, b) the major (ε_1) and the minor (ε_2) true strain distribution along the sheet. In the sheet center, the true strain values (ε_1) are about 0.15, gradually increasing up to 0.35 in the region between the punch pole and the die radius. From this region, the major true strain value diminishes up to the region of contact with the die (Fig. 4a).

Figure 4b shows the minor true strain distribution (ε_2). Note that the minor strains (ε_2) in the active region of the punch are of the same magnitude order as the major true strain (ε_1) in the region corresponding to the punch pole (Fig. 4a – ε_1 approx. 0.15). However, the strains distribution ε_2 along the path up to the blank holder is more homogeneous than that of ε_1, with no strain increases in the free contact area.

Like ε_1, the minor true strain is positive in the entire region of the formed sheet, which is in agreement to the experimental tests of Chemin Filho (2004) for this punch geometry and test specimen type. The positive ε_1 and ε_2 true strains must somehow be compensated so that the material volume remains constant. Thus, there is a decrease in the sheet's thickness, i.e., the true strain ε_3 along the sheet must be negative.

The results of the simulation were in agreement with the above. The true strain values found in the test specimen were negative along the entire strained sheet with their intensity increasing or decreasing in the same regions where ε_1 increased or decreased (Fig. 4c).

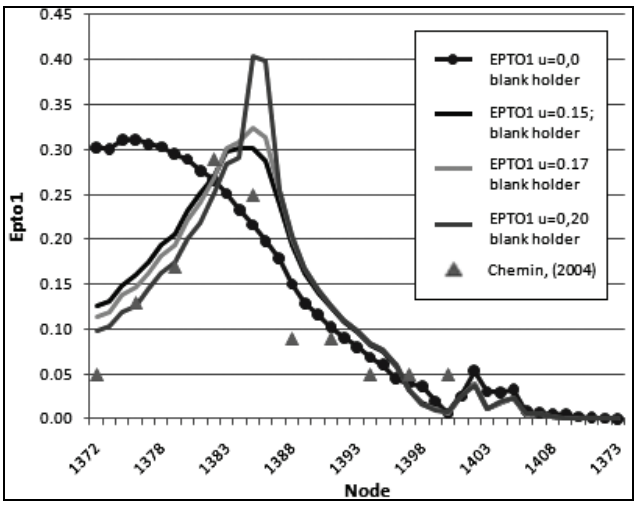

Figure 3. Major true strain distribution and the distance from the center of the hemispherical punch (Rp 50 mm) for different friction coefficient.

The decrease in thickness is also shown in Fig. 4d. The region of smallest thickness after forming corresponds to the one with the greatest ε_1 (considering absolute values).

Analysis of the True Strain Distribution with the Flat Punch (Rp 10 mm)

Figure 5 shows the major true strain in the direction from the die shoulder to the punch center (punch pole). The grid was refined in the region corresponding to the highest major strain deformation.

Note that at the end of curves, i.e., at the points corresponding to the die shoulder and the punch pole the simulation results are just below the experimental results (using the more refined grid). On the other hand, the unrefined grid shows a good agreement with the experimental results in the region of the punch radius (major true strain) and in the region between the punch and the die radii. It can be also noted that the grid with local refinement was able to reflect an inflection point of the experimental curve, as indicated in Fig. 5, which was not the case with the locally unrefined grid.

Figure 6a shows the major true strain distribution along the sheet, indicating the major strain region (identified as "MX"). Similarly, as can be seen, the true strain was quite low in most of the punch contact area. This was due to the action of the punch in a large region of the sheet imposing a greater strain restriction. Figure 6b also indicates that the region of the test specimen in contact with the punch shows minor true strain values (ε_2) varying from -0.026 to 0.050. Therefore, portions of the test specimen in the contact region with the punch are subjected to deep drawing, plane stress state and regions subjected to stretching, depending on the minor true strain value in that region.

Figure 6c shows the true strain in the thickness direction. Note that the deformation in the thickness is negative throughout the strained area, compensating the true strains ε_1 and ε_2.

The reduction in thickness is also illustrated in Fig. 6d, which shows the thickness distribution along the sheet. As can be seen, the thickness reduction occurs starting from the die shoulder. The maximum value of this reduction occurs in the region corresponding to the punch radius. The sheet thickness is practically uniform, but also thinner than the initial thickness in the region under the punch.

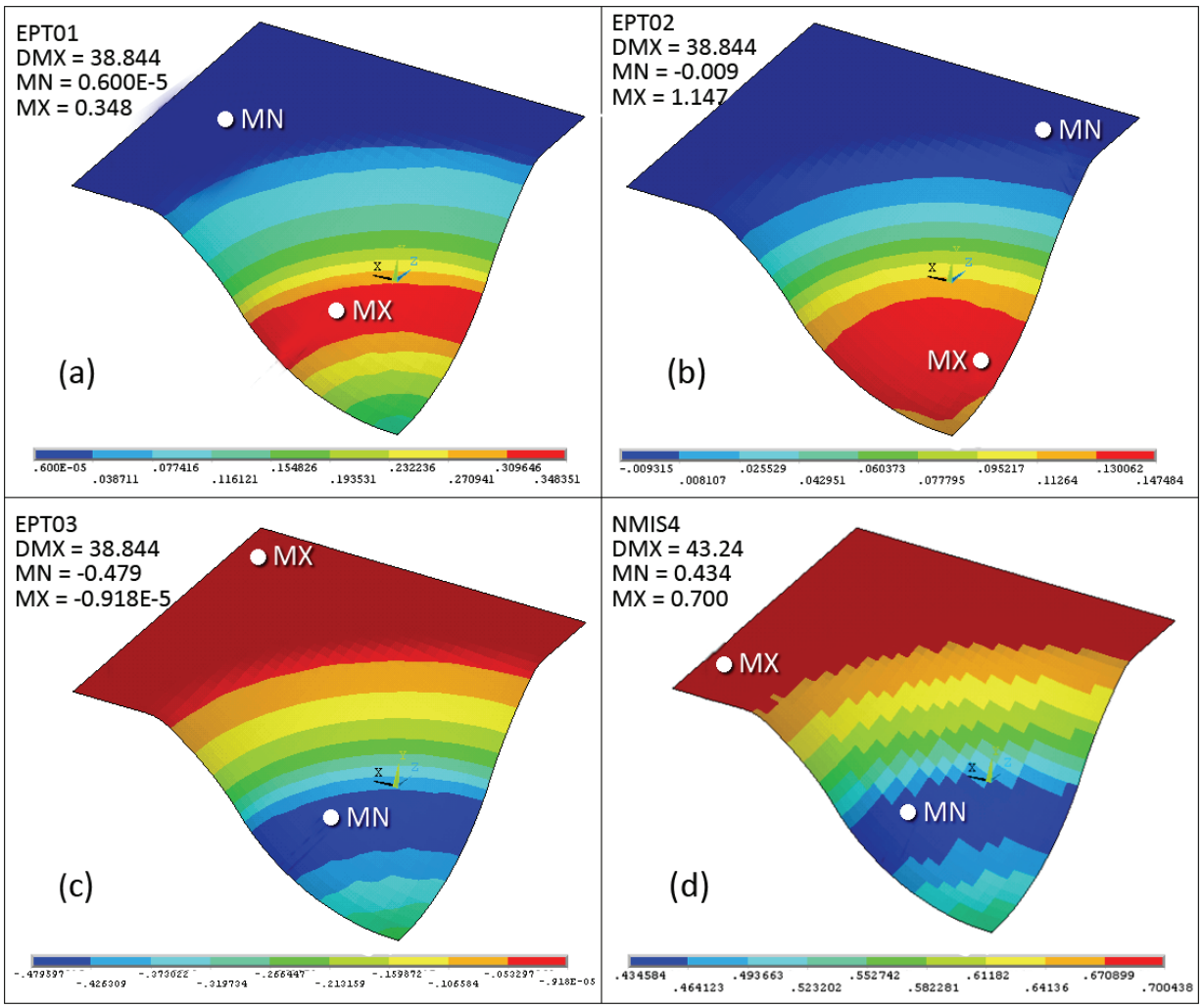

Figure 4. The true strain and thickness distribution as a function of distance from the center of the hemispherical punch (Rp 50 mm): a) major true strain, b) minor true strain, c) thickness true strain and d) thickness distribution (mm).

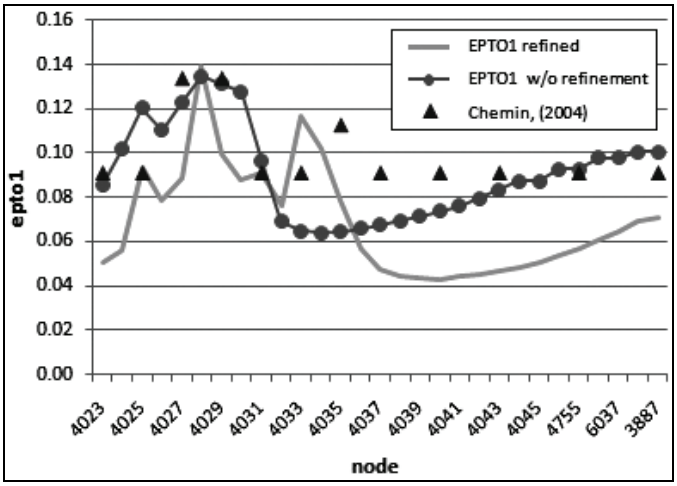

Figure 5. The true strain distribution comparison and the experimental data for the flat punch (Chemin Filho, 2004).

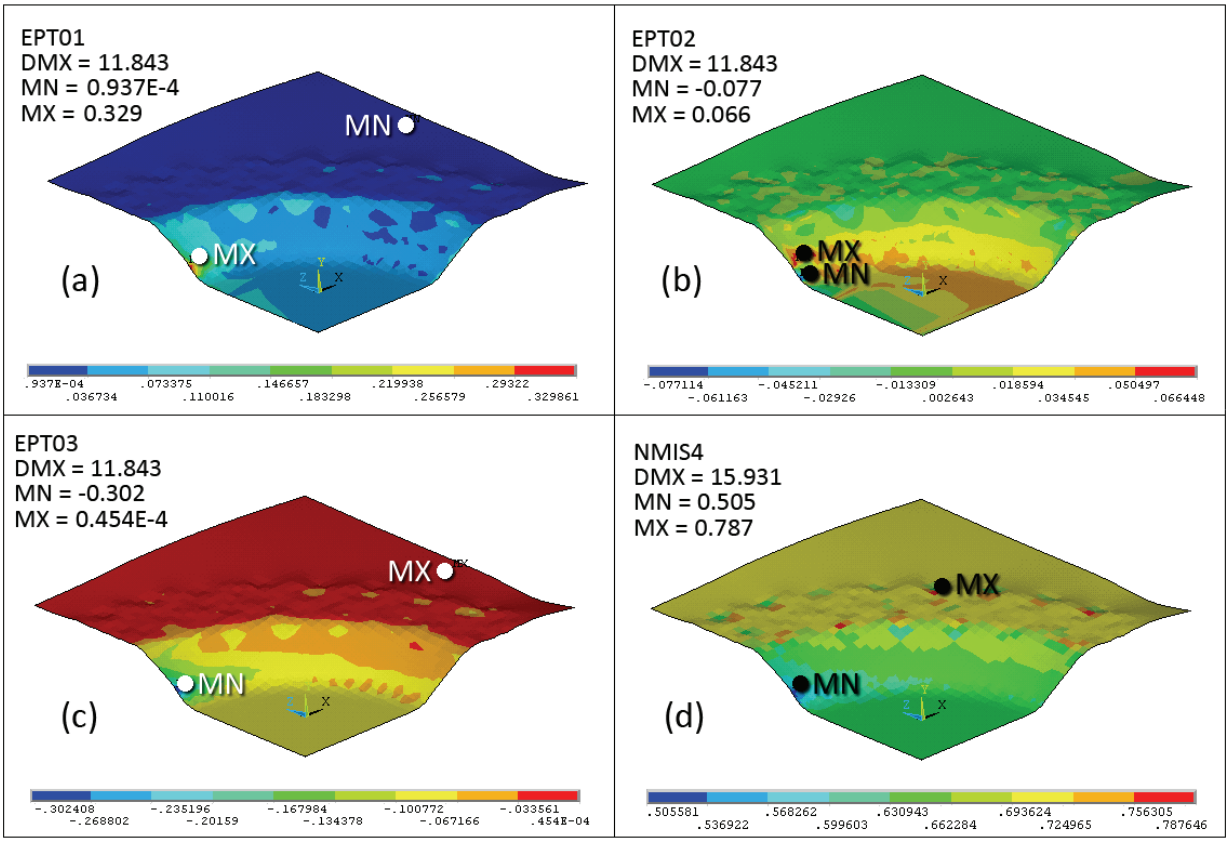

Figure 6. The true strain and thickness distribution as a function of distance from the center of the flat punch (Rp 10 mm): a) major true strain and refined grid, b) minor true strain, c) thickness true strain and d) thickness distribution (mm).

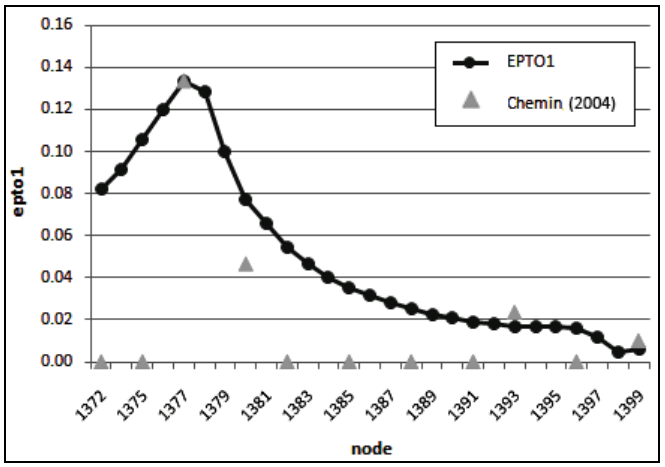

Figure 7. Major true strain distribution using the deep-ellipse punch (Rp 25 mm) (Chemin Filho, 2004).

Analysis of the true strain distribution using the deep-ellipse punch (Rp 25 mm)

The 25 mm radius punch was simulated using the same parameters as those employed to simulate the 50 mm radius punch, i.e., a grid without local refinement, with 2.5 mm sized elements and a 0.15 friction coefficient. Figure 7 shows the major true strain obtained by Chemin Filho (2004) and the simulation results.

The simulation data presented a good agreement to the experimental results, with the maximum true strain points coinciding in magnitude and location, as well as the shape of the curve. The Chemin Filho's (2004) experimental results showed values of zero for the major true strain (ε_1) in the region corresponding to the center of the punch (punch pole) and after the maximum true strain region. On the other hand, the simulated values started at 0.08 in the center of the punch, gradually declining to 0.02 in the region between the highest value and the die radius. A possible explanation for this difference is that the experimental data reading method is limited by the resolution of the measurement system used, which was probably not able to detect oscillations in the deformation values below 0.02.

Figure 8a shows the major true strain value (ε_1) along the sheet. Note that the deformations are concentrated in the punch contact region, and decline to values close to zero along a few millimeters, causing a high strain gradient.

Figure 8b shows the minor true strain distribution (ε_2) along the sheet. The highest strain values were also located in the sheet's central region, which corresponds to the punch contact region. These values varied from 0.06 to negative values in the region between the die radius and the region of punch contact.

In the region of contact with the die radius, the deformation values were negative and close to zero. Thus, the sheet's strain state varied between stretching in its central region and in contact with the punch, shifting gradually to the plane strain state up to the region of contact with the die, where the predominant mechanism is deep drawing.

The true strain along the thickness (ε_3) is shown in Fig. 8c. As for the values of ε_2, the values of ε_3 in the region of contact with the die were close to zero in most of the contact area, presenting some isolated regions with higher values of around -0.02.

The sheet's strain states are also illustrated in Fig. 8d, which indicates the sheet's thickness after forming.

Stretching in the sheet's central region became evident by the decrease in the original thickness of 0.7 mm to values ranging from 0.58 mm to 0.61 mm in the punch contact region. In this region, the thickness reduction compensates the true strain state, which is positive in both main directions.

In the region between the die radius and the beginning of punch contact, the thickness values were slightly lower, varying from 0.61 mm to 0.69 mm. In this region, the thickness decrease compensates principally the major true strain. On the other hand, in the region of the die contact most of the sheet showed little thickness alteration.

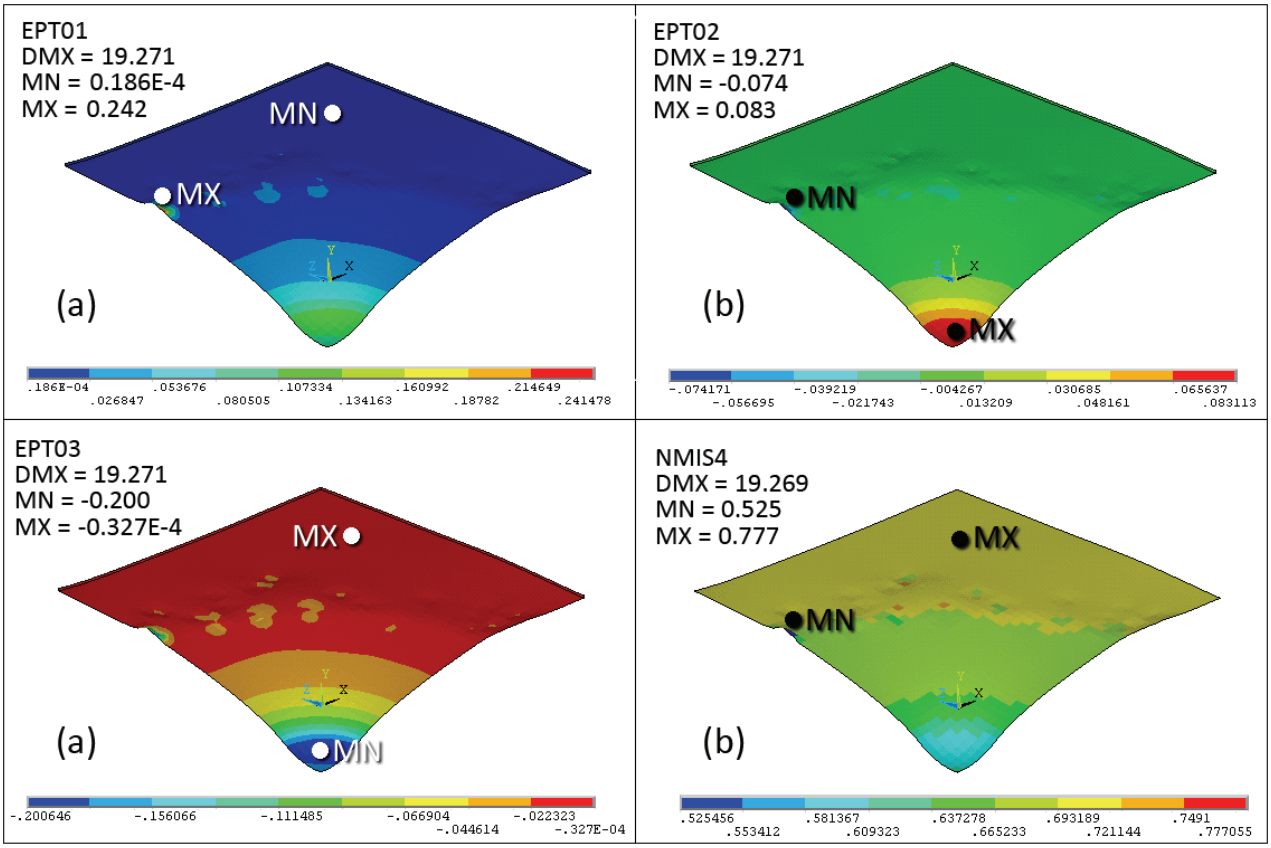

Figure 8. The true strain distribution and thickness as a function of distance from the center of the deep-ellipse punch (Rp 25 mm): a) major true strain, b) minor true strain, c) thickness true strain and d) thickness distribution (mm).

Conclusion

From the comparison between the experimental and simulated data, it can be concluded that the true strain analysis via the Finite Element Method using ANSYS 9.0/LS_Dyna software reproduces the experimental results satisfactorily. Qualitatively, it can be stated that the shape of the simulated and experimental curves are fairly similar to each other.

The greatest dispersions between the simulated and experimental results occurred in the cases involving the flat punch.

The use of the friction coefficient significantly changes the simulation results. With zero friction, the major true strain occurred in the central region of the test specimen, gradually decreasing up to the region of contact with the die. The use of a friction coefficient other than zero, on the other hand, restricted the true strain in the punch contact region. Thus, for the frictions range studied here, we can state that the major true strain in the punch contact region decreased as the friction coefficient increased.

In the contact region between the die and sheet and the punch and sheet, the strain intensity increased as the friction coefficient increased. In contrast, in the area after the major true strain region, the results were not significantly altered when the friction coefficient was modified.

The punch velocity used here was approximately 400 times bigger than the forming velocity (1.33 mm/s) used by Chemin Filho (2004), allowing for a considerable simulation time reduction. Because the results were in large part congruous with the experimental results, we can state that this hypothesis did not alter the results sufficiently to cause significant divergence from the experimental results. Mamalis et al. (1997) reported that higher velocities than the real ones can be used in explicit dynamic analyses. The necessary condition to use higher velocities is that the kinetic energy remains below a certain level so that the dynamic effect does not affect the simulation (Moreno, 2000).

Acknowledgments

The authors are indebted to the company ESSS and to Mr. Nicolau Botelho for the temporary supply of ANSYS 9.0/LS_DYNA software.

References

Abrantes, J.P., Batalha, G.F., 2003, "Modelagem da conformação de chapas metálicas por pressão hidrostática (bulge test)", In VI Conferencia Nacional de Conformação de Chapas, Porto Alegre, RS, Brazil, pp. 13-26.

Barlat, F. and Lian, J., 1989, "Plastic behavior and stretchability of sheet metals – Part1: a yield function for orthotropic sheets under plane stress conditions", *International Journal of Plasticity*, Vol. 5, pp. 51-66.

Borsoi, C.A., Hennig, R. and Schaeffer, L., 2000, "Novo teste tecnológico no LdTM para a melhor determinação da conformabilidade de chapas metálicas", III Conferencia Nacional de Conformação de Chapas, Porto Alegre, RS, Brazil, pp. 50-59.

Cao, J., Yao, H., Karafillis, A. and Boyce, M.C., 2000, "Prediction of localized thinning in sheet metal using a general anisotropic yield criterion", *International Journal of Plasticity*, Vol. 16, pp. 1005-1129.

Chemin Filho, R.A., 2004, "Avaliação das deformações de chapas finas e curvas CLC para diferentes geometrias de punções", Dissertação (Mestrado), Universidade Federal do Paraná, Curitiba, PR, Brazil.

Chemin Filho, R.A. and Marcondes, P.V.P., 2008, "Distribution of strain deformations in sheet metal using different punch geometries", *J. Braz. Soc. Mech. Sci. & Eng*., Vol. 30. No. 2, pp. 1-6.

Costa, A.R., 2003, "Análise da estampagem de chapas metálicas utilizando elementos finitos", Dissertação (Mestrado em Engenharia), Faculdade de Engenharia do Campus de Guaratinguetá, Universidade Estadual Paulista, Guaratinguetá, SP, Brazil.

Evangelista, S.H., 2000, "Diagramas de limite de conformação aplicados à análise por elementos finitos de um processo de estampagem em chapas metálicas", Dissertação (Mestrado), Escola de Engenharia de São Carlos, Universidade de São Paulo, São Carlos, SP, Brazil.

Gronostajski, J., Matuszak, A., Niechajowicz, A. and Zimniak, Z., 2004, "The system for sheet metal forming design of complex parts", *Journal of Materials Processing Technology*, Vol. 157-158, pp. 502-507.

Hallquist, J.O., 1998, "LS-DYNA3D Theoretical Manual", Livermore, Livermore Software Technology Corporation.

Hongzhi, D., Zhongqin, L., 2000, "Investigation of sheet metal forming by numerical simulation and experiment", *Journal of Materials Processing Technology*, Vol. 103, pp. 404-410.

Lobão, M.C., 2003, "Determinação de curvas limite de conformação por procedimentos experimentais e simulação numérica do processo de estampagem", Dissertação (Mestrado), Universidade Federal de Santa Catarina, Florianópolis, SC, Brazil.

Mamalis, A.G., Manolakos, D.E., Baldoukas, A.K., 1997, "Simulation of sheet metal forming using explicit finite element techniques: effect of material and forming characteristics – Part 2: Deep-drawing of square cups", *Journal of Materials Processing Technology*, Vol. 72, pp. 110-116.

Moreno, M.E., 2000, "Desenvolvimento e implementação de metodologia de otimização da geometria do blank em processos de conformação de chapas metálicas", Dissertação (Mestrado), Escola de Engenharia de São Carlos, Universidade de São Paulo, São Carlos, SP, Brazil.

Nakazima, K., Kikuma, T. and Hasuka, K., 1968, "Study on the formability of steel sheets", Yawata Technical Report No. 284, pp. 140-141.

Sampaio, A.P., Martins, C.A. and Souza, P.C., 1998, "Caracterização da conformabilidade de aço livre de intersticiais – IF – produzido via recozimento em caixa na Companhia Siderúrgica Nacional", I Conferência Nacional de Conformação de Chapas, Porto Alegre, RS, Brazil, pp. 89-100.

Yao, H. and Cao, J., 2002, "Prediction of forming limit curves using an anisotropic yield function with prestrain-induced backstress", *Int. J. Plast.*, Vol. 18, pp. 1013-1038.